Potential of erlotinib cyclodextrin nanosponge complex to enhance solubility, dissolution rate, in vitro cytotoxicity and oral bioavailability

DOI: https://doi.org/10.1016/j.carbpol.2015.10.080

Potential of erlotinib cyclodextrin nanosponge complex to enhance solubility, dissolution rate, in vitro cytotoxicity and oral bioavailability

Chander Parkash Dora[a,b,1], Francesco Trotta[c,1], Varun Kushwah[b], Naresh Devasari[a], Charan Singh[a], Sarasija Suresh[ad*], Sanyog Jain[b**]

[a] Department of Pharmaceutical Tech. (Formulations), National Institute of Pharmaceutical Education and Research (NIPER), S.A.S. Nagar, Punjab 160062, India

[b] Centre for Pharmaceutical Nanotechnology, Department of Pharmaceutics, National Institute of Pharmaceutical Education and Research (NIPER), S.A.S. Nagar, Punjab 160062, India

[c] Dipartimento di Chimica, Università degli Studi di Torino, Via P. Giuria, 7-10125, Torino, Italy

[d] Drug Design and Development Centre, Faculty of Pharmacy, MSR University of Applied Sciences, Bangalore, Karnataka 560054, India

∗ Corresponding author.

∗∗ Corresponding author at: Centre for Pharmaceutical Nanotechnology, Department of Pharmaceutics, National Institute of Pharmaceutical Education and Research (NIPER), S.A.S. Nagar, Punjab 160062, India. Tel.: +91 1722292055.

[1] These authors contributed equally to this work.

Highlights

- ERL-NS complex was prepared in 1:4 w/w ratio for the solubility enhancement.
- Complexation phenomenon was confirmed with DSC, PXRD, FTIR, etc.
- Oral bioavailability of ERL was also increased with nanosponge complex.
- Different cell line experiments showed the higher cytotoxicity of ERL-NS.

Keywords

Erlotinib; Tyrosine kinase inhibitor; Nanosponge; Solubility enhancement; In vitro cytotoxicity; Oral bioavailability

Abstract

The present study was envisaged to evaluate the effect of erlotinib β-cyclodextrin nanosponge (ERL-NS) on the solubility, dissolution, in vitro cytotoxicity and oral bioavailability of erlotinib (ERL). Preliminary studies were conducted to select the optimized stoichiometry concentration of ERL and NS. The drug nanosponge complex comprising of 1:4 proportions of ERL and NS was prepared by freeze drying. ERL-NS formed nanoparticles of 372 ± 31 nm size with narrow size distribution (0.21 ± 0.07 PDI) and high zeta potential

(−32.07 ± 4.58 mV). The complexation phenomenon was confirmed by DSC, SEM, PXRD, FTIR, and TEM studies. In vitro dissolution studies revealed an increased dissolution rate (2-folds) with an enhanced dissolution efficiency of the nanosponge complex in comparison to pure drug. In vitro cytotoxicity study and apoptosis assay in pancreatic cell lines (MIA PaCa-2 and PANC-1) indicates the increased toxicity of ERL-NS. Both, quantitative and qualitative cell uptake studies unveiled the higher uptake efficiency of ERL-NS than free drug. ERL-NS showed enhanced oral bioavailability with 1.8-fold higher C_{max} (78.98 ± 6.2 vs. 42.36 ± 1.75 μg/ml), and ∼2-fold $AUC_{0-\infty}$ (1079.95 ± 41.38 vs. 580.43 ± 71.91), in comparison to pure ERL. Therefore, we conclude that the formation of a complex of nanosponge with ERL is a successful approach to increase its solubility, dissolution and oral bioavailability which may ultimately result in reduction in dose and dose related side-effects.

Chemical compounds studied in this article

Erlotinib hydrochloride (PubChem CID: 176871); β-Cyclodextrin (PubChem CID: 444041); Ammonium acetate (PubChem CID: 517165); Atorvastatin (PubChem CID: 60823); Carbonydiimidazole (PubChem CID: 68263); Coumarin-6 (PubChem CID: 100334)

1. Introduction

The tyrosine kinase inhibitors are newer and novel class of anticancer drugs, predominantly for pancreatic cancer. Erlotinib hydrochloride (ERL; Fig. 1(I)), a USFDA approved drug approved initially for non-small cell lung cancer, is an epidermal growth-factor receptor (EGFR) tyrosine kinase inhibitor. Its potential for treatment of various other cancers such as breast cancer, locally advanced or metastatic non-small cell lung cancer (Vrignaud, Hureaux, Wack, Benoit, & Saulnier, 2012), ovarian cancer, glioma, head and neck cancer, and colorectal cancer has also been demonstrated (Dowell et al., 2005, Liversidge and Jenkins, 2012a). ERL competes with ATP in a reversible way, for binding to the adenosine triphosphate (ATP) binding site of the receptor. The receptor undergoes dimerization when ERL binds to its extracellular domain. This dimerization further activates tyrosine kinase domain intracellularly, which further autophosphorylates the critical tyrosine residues on the cytoplasmic terminal (Latha et al., 2013).

ERL has poor bioavailability when administered through oral route, mainly due to its poor biopharmaceutical characteristics (poor solubility, instability in gastrointestinal environment) and high first-pass metabolism. There are several dose-limiting side effects associated with ERL including acniform rashes, mucositis, diarrhea, and hematological side effects such as anemia, thrombopenia and neutropenia (Marslin et al., 2009). Thus, there is an urgent requirement of a formulation with high solubility, bioavailability and low toxicity for patient compliance.

An improved dissolution rate and solubility of ERL could result in enhanced bioavailability and therefore could possibly minimize the dose-related adverse effects. Various approaches have been evaluated to overcome the challenges associated with ERL therapy exemplified by cyclodextrin complex (Devasari et al., 2015), reverse micelle loaded lipid nanoparticles (Vrignaud et al., 2012), poly (d,l-lactic-co-glycolic acid) nanoparticles (Marslin et al., 2009), hybrid nanoparticles (Jesson et al., 2014), liposomes (Morton et al., 2014, Trummer, 2010), and other types of nanoparticles (Liversidge and Jenkins, 2012a, Liversidge and Jenkins, 2012b). In this regard, there exists immense potential of complexing therapeutic active constituents with nanosponges for improving oral bioavailability and therapeutic efficacy (Hüsch et al., 2011, Maiti et al., 2007, Wei et al., 2010, Yanyu et al., 2006).

The cyclodextrin-based nanosponges (NS) are hyper cross-linked sponge-like, polymeric structures, derived from β-cyclodextrins with a high capacity to interact with small molecules in its matrix (Torne, Ansari, Vavia, Trotta, & Cavalli, 2010). The NS can be obtained by crosslinking different types of cyclodextrin using carbonyldiimidazole, pyromellitic dianhydride and diphenyl carbonate cross-linkers (Ansari, Vavia, Trotta, & Cavalli, 2011). It exhibits high solubilizing efficiency of hydrophobic drug molecules and they are proposed to form inclusion and non-inclusion complexes with different drugs. Drug-loaded NS when dispersed in aqueous vehicle forms colloidal nanosuspension with a tendency to extend drug release (Swaminathan et al., 2010).

Here, in the present study, we developed β-cyclodextrin based nanosponge of erlotinib hydrochloride (ERL-NS) and evaluated its impact on solubility, dissolution, in vitro cytotoxicity in pancreatic cell lines and oral bioavailability.

2. Materials and methods

2.1. Materials

Erlotinib hydrochloride (ERL) was a kind gift from Mac-Chem Products (India) Pvt. Ltd. (Mumbai, India). Sodium hydroxide, sodium chloride, potassium chloride, potassium hydrogen phosphate, disodium hydrogen phosphate, Potassium dihydrogen phthalate and n-octanol were purchased from HiMedia labs (Mumbai, India). Dulbecco's modified Eagle's medium (DMEM), antibiotic–antimycotic solution, 3 (4,5-dimethylthiazol-2-yl)-2,5-diphenyltetrazolium bromide (MTT), ethylenediamine-tetra acetic acid (EDTA), trypsin and sodium acetate were purchased from Sigma–Aldrich Co., St. Louis, MO, USA. Fetal bovine serum (FBS) was procured from Invitrogen™, life technologies, Thermo Fisher Scientific Inc. (USA). High-Performance Liquid Chromatography (HPLC) grade reagents such as acetonitrile and methanol were obtained from J.T. Baker (USA). Ammonium acetate was purchased from Merck & Co., Inc. (Mumbai, India). MIA PaCa-2 and PANC-1 (Human pancreas adenocarcinoma) cell lines were obtained from the cell repository facility of National Centre for Cell Sciences (NCCS), Pune, India. All other chemicals used were of analytical grade.

2.2. Synthesis of β-cyclodextrin nanosponge

Synthesis of β-cyclodextrin nanosponge was detailed in the previous work (Shende et al., 2015, Trotta and Tumiatti, 2002). Briefly, 17.42 g of anhydrous β-CD (15.35 mM) was added in 100 ml dimethylformamide (DMF) in round bottom flask under stirring until a clear solution was formed. Further, 9.95 g of cross-linker carbonyldiimidazole (CDI; 61.4 mM) was added in the same flask and kept the reaction at 100 °C for 24 h under magnetic stirring. Once the reaction was completed, the product is left to cool at room temperature, added excess of double distilled water, filtered, purified by prolonged Soxhlet extraction with ethanol, which was further dried in vacuum and grounded in mechanical milling. Anhydrous β-CD and CDI were taken in 1:4 molar ratios.

2.3. Preparation of erlotinib nanosponge complex

ERL-nanosponge complex (ERL-NS) was prepared by previously established freeze drying method (Ansari et al., 2011). Accurately weighed quantities of NS were suspended in 20 ml of HPLC grade water on a magnetic stirrer and to it, ERL was added in a w/w ratio of 1:2, 1:4 and 1:6 (drug: nanosponge). Further, this mixture was sonicated for 10 min and kept for 24 h under stirring. The suspension was centrifuged at 4000 rpm for 10 min to separate the uncomplexed drug and supernatant was freeze-dried using VirTis Lyophilizer (Wizard 2.0, USA). The condenser temperature was maintained at −60 °C temperature and pressure of 200 mT to

obtain drug-loaded NS formulation. Here, Trehalose (5 w/v%) was used as a cryoprotectant. The resultant complex was stored below 20 °C.

2.4. Determination of size, polydispersity index and zeta potential

Particle size, polydispersity index (PDI) and zeta potential of formulation were measured by photon correlation spectroscopy using Zetasizer Nano ZS 90 (Malvern Instruments, UK). The samples were suitably diluted with HPLC grade water before every measurement.

2.5. Solubility study

Solubility of ERL, physical mixture, and ERL-NS (obtained from different ratios of drug and NS) was determined by shake flask apparatus. Briefly, excess of ERL, physical mixture, and ERL-NS were added to HPLC grade water in sealed glass containers at 25 °C. The samples were agitated at100 rpm for 24 h in the shaker water bath (EQUITRON®, Medica Instrument Mfg. Co., India), then centrifuged at 10,000 rpm for10 min. The supernatants were filtered (0.45 µm PVDF syringe filter, Millipore Millex-HV). The filtrate was suitably diluted with methanol and analyzed by reverse phase HPLC consisting of a Waters 2695 Separations Module and a Water 2996 photodiode array detector (PDA) (Waters Co., MA, USA). A C18 Luna® RP-HPLC (250 mm × 4.6 mm, 5 µm) (Phenomenex Inc., CA, USA) analytical column was used for the estimation. The optimized mobile phase was composed of ammonium acetate buffer (pH 4.0) and acetonitrile (42:58 v/v), with 1 ml/min flow rate. Samples of 20 µl were analyzed for quantification of ERL at 247 nm using PDA detector.

2.6. Loading efficiency of ERL in ERL-NS

Accurately weighed amount of ERL (5 mg) loaded nanosponges were firstly dissolved in methanol, sonicated for 10 min, centrifuged properly, diluted suitably and analyzed by HPLC at 247 nm.

2.7. Differential scanning calorimetry (DSC)

Thermal characteristics of ERL, NS, physical mixture, and the nanosponge complex of ERL were analyzed using DSC (DSC 821e, Mettler-Toledo International Inc., Switzerland). Each sample (3–5 mg) was heated in a crimped aluminum pan between 25 °C and 300 °C at a scanning rate of 20 °C/min and under a nitrogen flow of 40 ml/min. Instrument was previously calibrated with empty pan for baseline and indium for heat rate.

2.8. Fourier transform infra-red spectroscopy (FTIR)

The FT-IR spectra of ERL, NS, their physical mixture, and the ERL-NS complex between 4000 cm^{-1} and 450 cm^{-1} (mid-infrared region) were obtained using a FTIR Synthesis Monitoring System (PerkinElmer® Inc., USA) equipped with Spectrum software. Each sample was prepared with a spectroscopic grade potassium bromide (KBr) powder and then pressed into 1 mm pellets (1 mg of sample per 100 mg dry KBr) using a press sheet.

2.9. X-ray diffraction studies (XRD)

Powder X-ray diffraction (XRD) patterns of ERL, NS, their physical mixture, and the ERL-NS were recorded with an X-ray diffractometer (D8 Advanced Diffractometer, Bruker AXS GmbH, Germany) employing Cu Kα

(wavelength 1.5406 Å, tubeoperated at 40 kV, 40 mA) at room temperature. Data was collected over an angular range from 4° to 40° 2θ at a step size of 0.01° and scan rate of one second. The obtained diffractograms were analyzed with DIFFRAC plus EVA (ver.9.0) diffraction software.

2.10. Scanning electron microscopy (SEM)

The surface morphologies of ERL and the nanosponge complex of ERL were examined using scanning electron microscope (Hitachi S-3400N, Hitachi High-Tech Co., Japan). Diluted ERL-NS with HPLC grade water and solid ERL were placed on an aluminum stub by a bioadhesive carbon tape and sputter-coated (E-1010, Hitachi High-Tech Co., Japan) with gold-palladium alloy to minimize the surface charging. The samples were examined using SEM at 10 kV.

2.11. Transmission electron microscopy (TEM)

The surface morphology of ERL-NS was studied by transmission electron microscope (FEI Tecnai G2F20, Netherlands). A sample of nanosponge complex was diluted (100×) with HPLC water. It was placed on the carbon-coated copper grid and stained with phosphotungstic acid (2 w/v%). Finally, the grid was air dried, and scanned with the transmission electron microscope at different magnifications.

2.12. In vitro drug release

The dissolution studies of the ERL and its nanosponge complex were performed in dissolution apparatus using the paddle method (USP 37 Type II, Electrolab TDT-08L, Mumbai, India). Briefly, the samples were individually placed in dissolution vessel containing 1000 ml of 0.1 N HCL, maintained at 37 ± 0.5 °C at 75 rpm. A 5 mg of pure drug and its equivalent amount of nanosponge complex were added to the dissolution medium. Samples were withdrawn at appropriate time intervals and replaced with same volume of fresh dissolution medium to maintain the sink conditions. The solution was immediately filtered through (0.45 µm PVDF syringe filter, Millipore Millex-HV), suitably diluted and analyzed by HPLC method as described previously. The dissolution efficiency (DE) was calculated according to Eq. (1) given below (Reddy, Rehana, Ramakrishna, Chowdary, & Diwan, 2004):

$$DE = \frac{\int_{t_1}^{t_2} y dt}{y_{100}(t_2 - t_1)} * 100\% \quad (1)$$

where y is the percent drug dissolved. DE is the area under curve between time points t1 and t2 expressed as a percentage of the curve at maximum dissolution, y100, over the same time period. It is preferable to choose a time interval corresponding to 70–90% dissolution unless one wishes to compare an early part of the dissolution curve. Normally $t_1 = 0$ for a formulation where there is no lag phase. In the current study $t_1 = 0$ and $t_2 = 60$ min.

2.13. In vitro cell culture experiments

2.13.1. Cell uptake

2.13.1.1. Qualitative uptake

Coumain-6 was used as a model tracing agent to evaluate the cellular uptake of drug in cell lines. Briefly, Coumarin-6 NS was prepared by freeze drying method (Ansari et al., 2011). Accurately weighed quantities of

NS were suspended in 20 ml of HPLC grade water on a magnetic stirrer and to it, Coumarin-6 was added in a w/w ratio of 1:4. Further, this mixture was sonicated for 10 min and kept for 24 h under stirring. The suspension was centrifuged at 4000 rpm for 10 min to separate the uncomplexed drug and supernatant was freeze-dried using VirTis Lyophilizer (Wizard 2.0, USA). The condenser temperature was maintained at −60 °C temperature and pressure of 200 mT to obtain Coumarin-6 NS. Here, Trehalose (5 w/v%) was used as a cryoprotectant. The resultant complex was stored below 20 °C.

MIA PaCa-2, PANC-1 cells were seeded at a density of 3,00,000 cells/well in 6 well plate (Costars, Corning Inc., NY, USA) and incubated overnight for cell attachment. The cells were then exposed to Coumarin-6 NS (equivalent to 1 µg/ml of Coumarin-6) for 2 h. Subsequently the medium was removed and cells were washed twice with the PBS (pH 7.4). The cells were fixed with glutaraldehyde (2.5 v/v%) (Sigma, USA), washed and observed under the confocal laser scanning microscopy (CLSM) (Olympus FV1000, Olympus Imaging America Inc., USA).

2.13.1.2. Quantitative uptake

MIA PaCa-2, PANC-1 cells were seeded at a density of 1,00,000 cells/well in 24 well cell culture plates (Costars, Corning Inc., NY, USA) and allowed to attach overnight. The cell culture medium was replaced with fresh medium containing varying concentration of free ERL, and ERL-NS and further incubated for 2 h to evaluate the concentration dependent effect on cell uptake. Upon completion of incubation period, the medium was removed and cells were washed twice with PBS (pH 7.4). Similarly, time dependent cell uptake studies were also performed by incubating the MIA PaCa-2, PANC-1 cells with appropriate concentration of different formulations for varying time intervals (0.5, 1, 1.5, 2, 4 h). Further cells were lysed with the 0.1% Triton X-100 followed by extraction with methanol to completely solubilize the internalized drug. The cell lysate was centrifuged (Sigma K 300, USA) at 21,000 rpm for 10 min and obtained supernatant was subjected to HPLC analysis for quantification of internalized drugs.

2.13.2. Cell cytotoxicity

The cell cytotoxicity of ERL-NS, free drug and blank NS was determined using MTT assay in MIA PaCa-2, PANC-1 (human pancreas adenocarcinoma) cell lines by following our previously reported protocol (Swarnakar, Thanki, & Jain, 2013). Briefly, cells were grown in Dulbecco's modified essential medium, accompanied with Earle's salts, l-glutamine, nonessential amino acids, sodium bicarbonate, sodium pyruvate, 10% FBS, 100 U/ml penicillin, and 100 mg/ml streptomycin and maintained under 5% CO2 atmosphere at 37 °C. Cells were harvested by using 0.25 w/v% trypsin–EDTA solution, sub-cultured in 96-well culture plate (Costars, Corning Inc., NY, USA) at a density of 104 cells/well and incubated with different equivalent concentrations (0.1, 1, 10 and 20 µg/ml) of ERL-NS, free drug and blank NS. The extent of viability of the cells is indicated by conversion of MTT to purple colored formazan by metabolically active cells. The cells were then solubilized with DMSO (dimethyl sulphoxide) and optical density of the released, solubilized formazan reagent was measured at 540 nm spectrophotometrically. The cell viability was evaluated by following equation:

$$Relative\ cell\ viability = absorbance\ of\ sample * \frac{100}{absorbance} of\ control$$

2.13.3. Apoptosis

The cell cytotoxicity potential of the ERL and ERL-NS were further assessed as a function of their capability to induce apoptosis in MIA PaCa-2 and PANC-1 cells. Standard phosphatidyl serine externalization assay based

on Annexin V binding was monitored to estimate the apoptosis (Jain, Thanki, & Jain, 2014). Briefly, MIA PaCa-2 and PANC-1cells were seeded at a density of 105 cells per well in the six-well tissue culture plate (Costars, Corning Inc., NY, USA) and allowed to attach overnight at 37 °C and 5% CO_2. The media was aspirated and cells were exposed fresh media containing ERL and ERL-NS, equivalent to 1 mg/ml and incubated for 6 h. After incubation, the cells were washed with PBS (2 times) and double stained with Annexin V Cy3.18 conjugate (AnnCy3) and 6-carboxyfluorescein diacetate (6-CFDA) following the manufacturer's protocol (Annexin V-Cy3™ Apoptosis Detection Kit, Sigma, USA). After that, these cells were visualized under CLSM with green (for 6-CFDA) and red (for AnnCy3) channels. The cells stained with different fluorescence were categorized as live (green), apoptotic (red and green) and necrotic (green). Apoptosis index, the ratio of the fluorescence intensity of the red fluorescence (originated from the Annexin V Cy3.18 conjugate, estimate of apoptosis) to the fluorescence intensity of green fluorescence (originated from the 6-carboxyfluorescein, estimate of viable cells) was also calculated for the ERL and ERL-NS. The quantitative evaluation of fluorescence within the images could be determined by processing images with Image J software (U.S. National Institutes of Health, Bethesda, Maryland, USA, http://imagej.nih.gov/ij/).

2.14. In vivo pharmacokinetics

The pharmacokinetics of ERL and ERL-NS were evaluated in a fasted SD rat model. Animals (Female Sprague Dawley (SD) rats) of 200–250 g were obtained from the central animal facility (CAF), NIPER, India. The study protocol was approved by the Institutional Animal Ethics Committee (IAEC), National Institute of Pharmaceutical Education and Research (NIPER), S.A.S Nagar, India. The animals were maintained at 25 ± 2 °C and 50–60% relative humidity under natural light/dark conditions for one week before the experiment.

Rats were divided into two groups (n = 5). A dose of 10 mg/kg dose of ERL was orally administered to one group while the other group received ERL-NS equivalent to 10 mg/kg of ERL. The animals were fasted overnight (at least 8 h before dosing). The individual dose was calculated based on body weights measured on the day of drug administration.

Blood samples were collected via retro-orbital venipuncture into heparinized tubes at regular time interval for upto 24 h. Blood samples were centrifuged at 10,000 rpm for 10 min. The plasma samples were collected and stored at −20 °C until analyzed.

The plasma samples were analyzed for ERL concentrations using in-housed developed and validated reverse phase HPLC method. Briefly, 50 µl of internal standard solution (Atorvastatin, 5 µg/ml) was added to 200 µl of plasma aliquots containing ERL and then vortexed for 60 s. Further, 200 µl of a mixture of methanol: acetonitrile (3:1) was added to precipitate proteins, vortexed for 5 min and then centrifuged at 10,000 rpm for 10 min. The supernatants were separated, filtered and analyzed for drug content by validated HPLC method. Calibration curves were plotted for the concentration range of 10–1000 ng/ml (R^2 0.959). Mobile phase employed for analysis was the mixture of methanol and ammonium acetate buffer (pH 4) (73:27 v/v) at flow rate of 1.2 ml/min. Retention time of ERL and atorvastatin was found to be 5.05 and 5.95 min respectively. The detection wavelength (λ_{max}) set for ERL was at 247.

2.15. Pharmacokinetic data analysis

The pharmacokinetic parameters of ERL-NS were calculated by Kinetica software version 5.0 (Thermo Fisher Scientific Inc., USA), and compared with free ERL. Maximum concentration (C_{max}) and time to reach maximum concentration (T_{max}) are the values obtained directly from concentration–time curve. Area under the concentration–time curve ($AUC_{0-\infty}$), elimination half-life ($t_{1/2}$), mean residence time (MRT) were determined.

2.16. Statistical analysis

All the results are exhibited here, as mean ± standard deviation (SD). Data was analyzed using Student's t-test or one-way ANOVA (GraphPad InStat Software Demo, US); p-values <0.0001 was considered as statistically extremely significant.

3. Results and discussion

Erlotinib is a potent tyrosine kinase inhibitor which belongs to BCS II class (O'Brien & Fallah Moghaddam, 2013). Poor solubility of drugs always remains a huge challenge for formulation scientists. Moreover, a high dose of ERL is required to be administered which may further increase dose related toxicity. In the current study, we utilized previously synthesized and characterized nanosponge based on the reaction between β-cyclodextrin monomer and CDI cross-linker (Castiglione et al., 2013, Shende et al., 2015, Swaminathan et al., 2010, Trotta and Cavalli, 2009, Trotta and Tumiatti, 2002, Trotta et al., 2012). Furthermore, the nanosponge was utilized to prepare its inclusion complex with ERL with an aim to enhance its solubility, dissolution rate and thus its oral bioavailability. In our previous study (Devasari et al., 2015), we have already found the favorable interactions (K_α = 211 M^{-1}, which also supports the findings of Loftsson, Jarho, Masson, and Järvinen (2005)) between the β-cyclodextrin (basic unit of nanosponge) and ERL by different experiments, e.g. phase solubility study, ^{1}H NMR and molecular modeling, etc., which also validates the inclusion phenomenon between nanosponge and free drug.

Preliminary phase solubility studies in purified water of ERL-NS composed of different w/w ratios of drug and nanosponge is presented in Fig. 1(II). The solubility of all the nanosponge complexes were significantly higher ($p < 0.01$) than pure ERL (3.16 ± 0.73 μg/ml). The solubility of ERL was optimum in 1:4 w/w proportions of drug and NS. Further increase in drug and NS ratio did not enhance the solubility probably due to saturation solubility of drug in NS (Ansari et al., 2011). Hence, we selected formulation with 1:4 w/w ratio for further studies. The observed increase in solubility could be due to inclusion of the drug within the lipophilic sites present within the nanosponge network (Cavalli, Trotta, & Tumiatti, 2006).

The average particle size of selected ERL-NS was 372 ± 31 nm with unimodal particle size distribution (PDI = 0.21 ± 0.07). The zeta potential of the nanosponge complex was calculated by Henry equation was −32.07 ± 4.58 mV (Jiang, Han, & Hsieh, 2013). This high zeta potential value indicates sufficient stability of ERL-NS when dispersed in aqueous medium (Kobayashi, Wei, Iida, Ijiro, & Niikura, 2014). The zeta potential remained constant with insignificant difference (−30.83 ± 5.27 mV) ($p > 0.05$) when stored at 4 °C for 3 months. The loading efficiency of ERL in the nanosponge complex was considerably high (74.29 ± 6.81%) to confirm the high inclusion phenomenon between ERL and NS.

3.1. Solid state characterization of ERL-NS

Fig. 1(III) presents the DSC thermograms of ERL, NS, the physical mixture and ERL-NS. DSC thermogram of ERL exhibited a sharp endotherm at 235.98 °C, which corresponds to the melting endotherm of the drug. This type of endotherm was supported by prior art (Westheim, 2013). The physical mixture of ERL and NS exhibited a shift in the characteristic peaks of nanosponge and ERL. It may be assumed that during physical mixing there is a rise in the surrounding temperature resulting in the melting of the nanosponge in which ERL has dissolved partly forming the complex and eliciting an endotherm at lower temperature (122.18 °C). The thermogram of the nanosponge complex exhibits a single peak at 84.7 °C, which differs from the peak of ERL and nanosponge. It is evident that the original peaks of ERL and nanosponge disappear from the thermogram

of the complex and the phase transition temperature is lower than that of nanosponge which confirmed the occurrence of inclusion phenomenon between the two components (Ansari et al., 2011).

Fig. 1(IV) presents the FT-IR spectra of ERL, NS, physical mixture and the nanosponge complex, ERL-NS The spectrum of ERL exhibited strong absorption bands at 3012 cm^{-1} (for the CH_3, C-H stretching vibrations), 1634 cm^{-1} (for the NH, secondary amine bending vibrations), 3271 cm^{-1} (for the $\equiv$C-H stretching vibrations), 1243 cm^{-1}, 1075 cm^{-1} (for the phenyl ether group) and 1021 cm^{-1} (for the aliphatic ether group), which was also reported earlier (Parthasaradhi, Rathnakar, Raji, Muralidhara, & Srinivasa, 2010). The IR spectra of the nanosponge was characterized by the strong absorption bands at 3421 cm^{-1} (for the O-H stretching vibrations typical to carbohydrates), 1731 cm^{-1} (for the carbonate bond vibrations which also confirms the cyclodextrin based structure), 2928 cm^{-1} (for C-H stretching), 1467 cm^{-1} and 1032 cm^{-1} bands (for C-H bending and C-O stretching vibrations, respectively) (Darandale & Vavia, 2013). FT-IR spectrum showed the interactions between ERL and nanosponge that were evident from peak broadening and peak disappearance of characteristic peak. The physical mixture had superposition of the spectra of both ERL and NS and displayed no shift or very slight shift of the absorption band at 3277.10 cm^{-1} and 1633.83 cm^{-1}. While, the bands at 2899 cm^{-1} and 1478 cm^{-1} displayed a significant shift. Thus, physical mixture of ERL and NS exhibited few interactions between the nanosponge and the drug. However, the characteristic bands of ERL and NS (3271.42 cm^{-1} and 1731.57 cm^{-1}, respectively) was disappeared in ERL-NS. The spectrum of the complex showed comparative changes in center-frequencies (1638.37 cm^{-1} and 3418.38 cm^{-1}) widths of the characteristic absorption peaks, and thus confirmed the formation of a new type of interaction between the ERL and NS. These results indicated that the ERL formed a physical complex with NS (Lembo et al., 2013).

Fig. 1(V) presents the PXRD patterns of ERL, NS, their physical mixture and ERL-NS. The PXRD pattern of ERL showed the presence of intense, sharp peaks at 6.26, 9.43, 16.91, 20.02, 21.03, 22.29 and 25.08 on 2θ scale which indicated its crystalline behavior. The PXRD pattern of NS showed no sharp peaks which indicate its amorphous state. The physical mixture of both components showed crystalline peaks of ERL with reduced intensities. These findings suggested some interactions between ERL and NS. However, PXRD pattern of ERL-NS was very similar to pure NS pattern except for a few shifted peaks (e.g. 31.81 at 2θ scale) with reduced intensities. Thus, PXRD studies suggested the absence of crystallinity of drug in the ERL-NS which is absent in the physical mixture.

3.2. Morphology of ERL-NS

Fig. 2(I) represents the SEM images of ERL and the ERL-NS complex. ERL exhibited plate-shaped crystals. However, SEM image of ERL-NS complex showed spherical shape with complete loss of its characteristic plate shape which further indicated the inclusion phenomenon between drug and nanosponge. The TEM images of ERL-NS (with different magnifications) were illustrated in Fig. 2(II). ERL-NS appeared as uniform spherical morphology unaffected with drug encapsulation. The particle size obtained with TEM is almost similar with the size obtained by Zetasizer (~350–500 nm).

3.3. In vitro drug release

Fig. 3(I) depicts the in vitro dissolution profile of pure ERL and ERL-NS complex. From the release profile of drug and formulation, it was clearly evident that the significant higher and faster release of ERL-NS than ERL alone. The release profile of ERL-NS displayed 71.26 ± 0.54% drug release in 60 min; almost 2-fold higher release when compared to pure ERL (36.21 ± 5.09%). From the in vitro dissolution studies, it was confirmed that ERL formed inclusion complex with nanosponge leading to its increased solubility. This phenomenon can be attributed to the solubilization effect of nanosponge complex. It could be due to loss in crystallinity,

particle size reduction up to the molecular level and hydrogen bonding between the drug and nanosponge, as well (Jadhav, Petkar, Pore, Kulkarni, & Burade, 2013).

Table 1 presents the dissolution efficiencies of drug and complex at 10 min (DE_{10}), 30 min (DE_{30}) and at 60 min (DE_{60}). The dissolution efficiency of ERL-NS was significantly higher than the free drug ($p < 0.01$), which can be attributed to the inclusion complexation of ERL in NS resulting in enhanced solubilization followed by further amorphization of the drug during the process of freeze drying (Trapani et al., 2000). Different release models (i.e. zero order, first order, second order, Higuchi, Hixon-Crowell, Weibull, Backer-Lonsdale and Korsemayer-Peppas) were applied and Higuchi ($R^2 = 0.989$) was found the most suitable model for the release pattern of ERL-NS, which showed its matrix type of release behavior.

3.4. Cell uptake studies

In qualitative uptake study, CLSM images of MIA-PaCa 2 and PANC-1 cells incubated with Coumarin-6-NS and free Coumarin-6 (1 µg/ml, 2 h) are shown in Fig. 4(I). As evident, significantly higher fluorescence was visible inside the cells following 2 h incubation with C-6 loaded NS, suggestive of efficient internalization of NS in MIA-PaCa 2 and PANC-1 cells (Lembo et al., 2013). Horizontal line analysis showed that green and white line overlapping in case of Coumarin-6-NS while in case free coumarin-6, no such overlapping was seen that indicated internalization of Coumarin-6-NS within the cells.

Fig. 4(II) shows time and concentration dependent uptake of ERL formulations by MIA-PaCa 2 and PANC-1 cells. The uptake of ERL-NS was progressively increased with increase in the incubation time. However, uptake of nanoparticles attained a plateau/decline phase after 2 h, which could be due to the saturation of receptors gained after 2 h (Jain et al., 2013, Trono et al., 2011). An insignificant ($p > 0.05$) change in the amount of ERL uptake was observed upon increasing the incubation time of ERL-NS beyond 2 h. At highest tested concentration (20 µg/ml), the uptake of ERL-NS was 5.4- and 5.6-fold higher as compared to free ERL in MIA-PaCa 2 and PANC-1 cells.

3.5. In vitro cytotoxicity and apoptosis

The in vitro cytotoxicity of ERL and ERL-NS was evaluated by incubating MIA PaCa-2 and PANC-1 pancreatic cells for 24 h, 48 h and 72 h and determining the cell viability using MTT assay (Fig. 5). The ERL-NS was found to be more cytotoxic against both MIA PaCa-2 and PANC-1 cells, when compared to free ERL. When incubated with MIA PaCa-2 and PANC-1 pancreatic cells, IC_{50} values of ERL-NS in each time frame (24 h, 48 h and 72 h) was found significantly higher than free ERL (Table 2). We have also determined the toxicity of the blank nanosponge on MIA PaCa-2 and PANC-1 cells and which was found to be nontoxic. Higher toxicity observed with ERL-NS might be due to more endocytotic uptake as it was compared with free ERL (De Jong & Borm, 2008), also due to efficient internalization (Lembo et al., 2013). It could also be due to cell permeability of molecule changes by high solubilization potential of nanosponges (Torne, Darandale, Vavia, Trotta, & Cavalli, 2013). The noted findings were further validated by the apoptosis assay (Fig. 6). The apoptotic index was observed to be higher in ERL-NS as compared to ERL alone, which supported the previous findings where apoptotic cell death was found higher with nanosponge formulation than free drug (Minelli et al., 2012). This outcome has similar pattern in both pancreatic carcinoma cells. The apoptotic index was 0.37 and 0.42 with ERL, which was increased to 0.79 and 0.82, against MIA-PaCa 2 and PANC-1 cell lines, respectively.

3.6. In vivo pharmacokinetics

Fig. 3(II) represents the plasma concentration v/s time profile of ERL-NS and the pure drug. Various pharmacokinetic parameters are tabulated in Table 3. Studies revealed that nanosponge formulation was efficient to increase the C_{max} and $AUC_{0-\infty}$ by 1.8 and ~2-folds, respectively.

The relative bioavailability of the complex was approximately 200% in comparison to pure ERL, which further confirmed the enhanced bioavailability of ERL-NS. These results indicated that complex had a much higher rate and extent of bioavailability compared to ERL suspension. These results were also in agreement of in vitro dissolution studies. The results also support the formation of supramolecular complex, where the drug forms an inclusion complex within the nanocavities which reduces particles size, increases solubility and dissolution rate thus facilitating absorption resulting in higher bioavailability (Rao, Bajaj, Khole, Munjapara, & Trotta, 2013). The increase in oral bioavailability could also be credited to avoidance of presystemic metabolism and the first pass hepatic metabolism of drug by incorporation of nanoparticles which contributes an alternate pathway of absorption (Jain et al., 2012, Smith et al., 2008).

4. Conclusion

Formulation of cyclodextrin based nanosponge was successfully developed and implemented to enhance solubility, dissolution efficiency, and thus oral bioavailability of erlotinib. The existence of nanocavities inside nanosponge and also due to inclusion phenomenon of cyclodextrin makes erlotinib to possess higher solubility with enhanced bioavailability. The developed nanosponge of drug also showed higher cyotoxicity against pancreatic adenocarcinoma cell lines, which further increases its potential. Therefore, we conclude that inclusion complex of nanosponge with ERL is a successful approach to increase its solubility and bioavailability, which, may result in a reduction in dose and dose related side-effects. Furthermore, a systematic study of therapeutic efficacy and toxicity is warranted to fully understand the potential of this formulation.

Acknowledgements

The authors are thankful to Mac-Chem Products (India) Pvt. Ltd. (Mumbai, India) for providing gift samples of Erlotinib hydrochloride. Authors are thankful to Director, NIPER, S.A.S. Nagar for providing the necessary infrastructure facilities. Chander Parkash and Varun Kushwah are also thankful to University Grants Commission (UGC), New Delhi and Council of Scientific & Industrial Research (CSIR), New Delhi, respectively, for financial assistance. The help and co-operation provided by Mr. Rahul Mahajan and Mr. Vinod, NIPER, S.A.S. Nagar for SEM and TEM analysis respectively, is duly acknowledged.

References

Ansari, K. A., Vavia, P. R., Trotta, F., & Cavalli, R. (2011). Cyclodextrin-based nanosponges for delivery of resveratrol: In vitro characterisation, stability, cytotoxicity and permeation study. AAPS PharmSciTech, 12(1), 279–286.

Castiglione, F., Crupi, V., Majolino, D., Mele, A., Panzeri, W., Rossi, B., et al. (2013). Vibrational dynamics and hydrogen bond properties of -CD nanosponges: An FTIR-ATR, Raman and solid-state NMR spectroscopic study. Journal of Inclusion Phenomena and Macrocyclic Chemistry, 75(3–4), 247–254.

Cavalli, R., Trotta, F., & Tumiatti, W. (2006). Cyclodextrin-based nanosponges for drug delivery. Journal of Inclusion Phenomena and Macrocyclic Chemistry, 56(1–2), 209–213.

Darandale, S., & Vavia, P. (2013). Cyclodextrin-based nanosponges of curcumin: Formulation and physicochemical characterization. Journal of Inclusion Phenomena and Macrocyclic Chemistry, 75(3–4), 315–322.

De Jong, W. H., & Borm, P. J. (2008). Drug delivery and nanoparticles: Applications and hazards. International Journal of Nanomedicine, 3(2), 133.

Devasari, N., Dora, C. P., Singh, C., Paidi, S. R., Kumar, V., Sobhia, M. E., et al. (2015). Inclusion complex of erlotinib with sulfobutyl ether- -cyclodextrin: Preparation, characterization, in silico, in vitro and in vivo evaluation. Carbohydrate Polymers, 134, 547–556. Dowell, J., Minna, J. D., & Kirkpatrick, P. (2005). Erlotinib hydrochloride. Nature Reviews Drug Discovery, 4(1), 13–14.

Hüsch, J., Dutagaci, B., Glaubitz, C., Geppert, T., Schneider, G., Harms, M., et al. (2011). Structural properties of so-called NSAID–phospholipid-complexes. European Journal of Pharmaceutical Sciences, 44(1), 103–116.

Jadhav, P., Petkar, B., Pore, Y., Kulkarni, A., & Burade, K. (2013). Physicochemical and molecular modeling studies of cefixime-l-arginine-cyclodextrin ternary inclusion compounds. Carbohydrate Polymers, 98(2), 1317–1325.

Jain, A. K., Thanki, K., & Jain, S. (2013). Co-encapsulation of tamoxifen and quercetin in polymeric nanoparticles: Implications on oral bioavailability, antitumor efficacy, and drug-induced toxicity. Molecular Pharmaceutics, 10(9), 3459–3474.

Jain, A. K., Thanki, K., & Jain, S. (2014). Novel self-nanoemulsifying formulation of quercetin: Implications of pro-oxidant activity on the anticancer efficacy. Nanomedicine: Nanotechnology, Biology and Medicine, 10(5), 959–969.

Jain, S., Kumar, D., Swarnakar, N. K., & Thanki, K. (2012). Polyelectrolyte stabilized multilayered liposomes for oral delivery of paclitaxel. Biomaterials, 33(28), 6758–6768.

Jesson, G., Brisander, M., Andersson, P., Demirbüker, M., Derand, H., Lennernäs, H., et al. (2014). Carbon dioxide-mediated generation of hybrid nanoparticles for improved bioavailability of protein kinase inhibitors. Pharmaceutical Research, 31(3), 694–705.

Jiang, F., Han, S., & Hsieh, Y.-L. (2013). Controlled defibrillation of rice straw cellulose and self-assembly of cellulose nanofibrils into highly crystalline fibrous materials. RSC Advances, 3(30), 12366–12375.

Kobayashi, K., Wei, J., Iida, R., Ijiro, K., & Niikura, K. (2014). Surface engineering of nanoparticles for therapeutic applications. Polymer Journal, 46(8), 460–468.

Latha, S., Thangadurai, S. A., Jambulingam, M., Sereya, K., Kamalakannan, D., & Anilkumar, M. (2013). Development and validation of RP-HPLC method for the estimation of Erlotinib in pharmaceutical formulation. Arabian Journal of Chemistry (in press)

Lembo, D., Swaminathan, S., Donalisio, M., Civra, A., Pastero, L., Aquilano, D., et al. (2013). Encapsulation of Acyclovir in new carboxylated cyclodextrin-based nanosponges improves the agent's antiviral efficacy. International Journal of Pharmaceutics, 443(1), 262–272.

Liversidge, G., & Jenkins, S. (2012). Nanoparticulate erlotinib formulations. EP1871345 B1.

Liversidge, G. G., & Jenkins, S. (2012). Nanoparticulate quinazoline derivative formulations. US8309133 B2.

Loftsson, T., Jarho, P., Masson, M., & Järvinen, T. (2005). Cyclodextrins in drug delivery. Expert Opinion on Drug Delivery, 2(2), 335–351.

Maiti, K., Mukherjee, K., Gantait, A., Saha, B. P., & Mukherjee, P. K. (2007). Curcumin–phospholipid complex: Preparation, therapeutic evaluation and pharmacokinetic study in rats. International Journal of Pharmaceutics, 330(1), 155–163.

Marslin, G., Sheeba, C. J., Kalaichelvan, V., Manavalan, R., Neelakanta Reddy, P., & Franklin, G. (2009). Poly (d,l-lactic-co-glycolic acid) nanoencapsulation reduces Erlotinib-induced subacute toxicity in rat. Journal of Biomedical Nanotechnology, 5(5), 464–471.

Minelli, R., Cavalli, R., Ellis, L., Pettazzoni, P., Trotta, F., Ciamporcero, E., et al. (2012). Nanosponge-encapsulated camptothecin exerts anti-tumor activity in human prostate cancer cells. European Journal of Pharmaceutical Sciences, 47(4), 686–694.

Morton, S. W., Lee, M. J., Deng, Z. J., Dreaden, E. C., Siouve, E., Shopsowitz, K. E., et al. (2014). A nanoparticle-based combination chemotherapy delivery system for enhanced tumor killing by dynamic rewiring of signaling pathways. Science Signaling, 7(325), ra44.

O'Brien, Z., & Fallah Moghaddam, M. (2013). Small molecule kinase inhibitors approved by the FDA from 2000 to 2011: A systematic review of preclinical ADME data. Expert Opinion on Drug Metabolism & Toxicology, 9(12), 1597–1612.

Parthasaradhi, R. B., Rathnakar, R. K., Raji, R. R., Muralidhara, R. D., & Srinivasa, R. T. (2010). Erlotinib hydrochloride polymorph Form A substantially free of polymorph Form B. EP2218713 A1.

Rao, M., Bajaj, A., Khole, I., Munjapara, G., & Trotta, F. (2013). In vitro and in vivo evaluation of β-cyclodextrin-based nanosponges of telmisartan. Journal of Inclusion Phenomena and Macrocyclic Chemistry, 77(1–4), 135–145.

Reddy, M. N., Rehana, T., Ramakrishna, S., Chowdary, K., & Diwan, P. V. (2004). β-Cyclodextrin complexes of celecoxib: Molecular-modeling, characterization, and dissolution studies. AAPS PharmSci, 6(1), 68–76.

Shende, P., Kulkarni, Y. A., Gaud, R., Deshmukh, K., Cavalli, R., Trotta, F., et al. (2015). Acute and repeated dose toxicity studies of different β-cyclodextrin-based nanosponge formulations. Journal of Pharmaceutical Sciences, 104(5), 1856–1863.

Smith, N., Baker, S., Gonzalez, F., Harris, J., Figg, W., & Sparreboom, A. (2008). Modulation of erlotinib pharmacokinetics in mice by a novel cytochrome P450 3A4 inhibitor BAS 100. British Journal of Cancer, 98(10), 1630–1632.

Swaminathan, S., Pastero, L., Serpe, L., Trotta, F., Vavia, P., Aquilano, D., et al. (2010). Cyclodextrin-based nanosponges encapsulating camptothecin: Physicochemical characterization, stability and cytotoxicity. European Journal of Pharmaceutics and Biopharmaceutics, 74(2), 193–201.

Swarnakar, N. K., Thanki, K., & Jain, S. (2013). Effect of co-administration of CoQ10-loaded nanoparticles on the efficacy and cardiotoxicity of doxorubicin-loaded nanoparticles. RSC Advances, 3(34), 14671–14685.

Torne, S., Darandale, S., Vavia, P., Trotta, F., & Cavalli, R. (2013). Cyclodextrin-based nanosponges: Effective nanocarrier for Tamoxifen delivery. Pharmaceutical Development and Technology, 18(3), 619–625.

Torne, S. J., Ansari, K. A., Vavia, P. R., Trotta, F., & Cavalli, R. (2010). Enhanced oral paclitaxel bioavailability after administration of paclitaxel-loaded nanosponges. Drug Delivery, 17(6), 419–425.

Trapani, G., Latrofa, A., Franco, M., Pantaleo, M. R., Sanna, E., Massa, F., et al. (2000). Complexation of Zolpidem with 2-hydroxypropyl-β-, methyl-β-, and 2-hydroxypropyl-γ-cyclodextrin: Effect on aqueous solubility, dissolution rate, and ataxic activity in rat. Journal of Pharmaceutical Sciences, 89(11), 1443–1451.

Trono, J. D., Mizuno, K., Yusa, N., Matsukawa, T., Yokoyama, K., & Uesaka, M. (2011). Size, concentration and incubation time dependence of gold nanoparticle uptake into pancreas cancer cells and its future application to X-ray drug delivery system. Journal of Radiation Research, 52(1), 103–109.

Trotta, F., & Cavalli, R. (2009). Characterization and applications of new hyper-cross-linked cyclodextrins. Composite Interfaces, 16(1), 39–48.

Trotta, F., & Tumiatti, W. (2002). Cross-linked polymers based on cyclodextrins for removing polluting agents. US20050154198 A1.

Trotta, F., Zanetti, M., & Cavalli, R. (2012). Cyclodextrin-based nanosponges as drug carriers. Beilstein Journal of Organic Chemistry, 8(1), 2091–2099.

Trummer, B. J. (2010). . pp. 169. Development of Nano-Liposomal Formulations of Epidermal Growth Factor Receptor Inhibitors and their Pharmacological Interactions on Drug-Sensitive and Drug-Resistant Cancer Cell Lines. ProQuest Dissertations and Theses (74-10E) State University of New York at Buffalo.

Vrignaud, S., Hureaux, J., Wack, S., Benoit, J.-P., & Saulnier, P. (2012). Design, optimization and in vitro evaluation of reverse micelle-loaded lipid nanocarriers containing erlotinib hydrochloride. International Journal of Pharmaceutics, 436(1), 194–200.

Wei, W., Shi, S.-J., Liu, J., Sun, X., Ren, K., Zhao, D., et al. (2010). Lipid nanoparticles loaded with 10-hydroxycamptothecin-phospholipid complex developed for the treatment of hepatoma in clinical application. Journal of Drug Targeting, 18(7), 557–566.

Westheim, R. J. (2013). Hydrates of erlotinib hydrochloride WO2008049645 A2.

Yanyu, X., Yunmei, S., Zhipeng, C., & Qineng, P. (2006). The preparation of silybin–phospholipid complex and the study on its pharmacokinetics in rats. International Journal of Pharmaceutics, 307(1), 77–82.

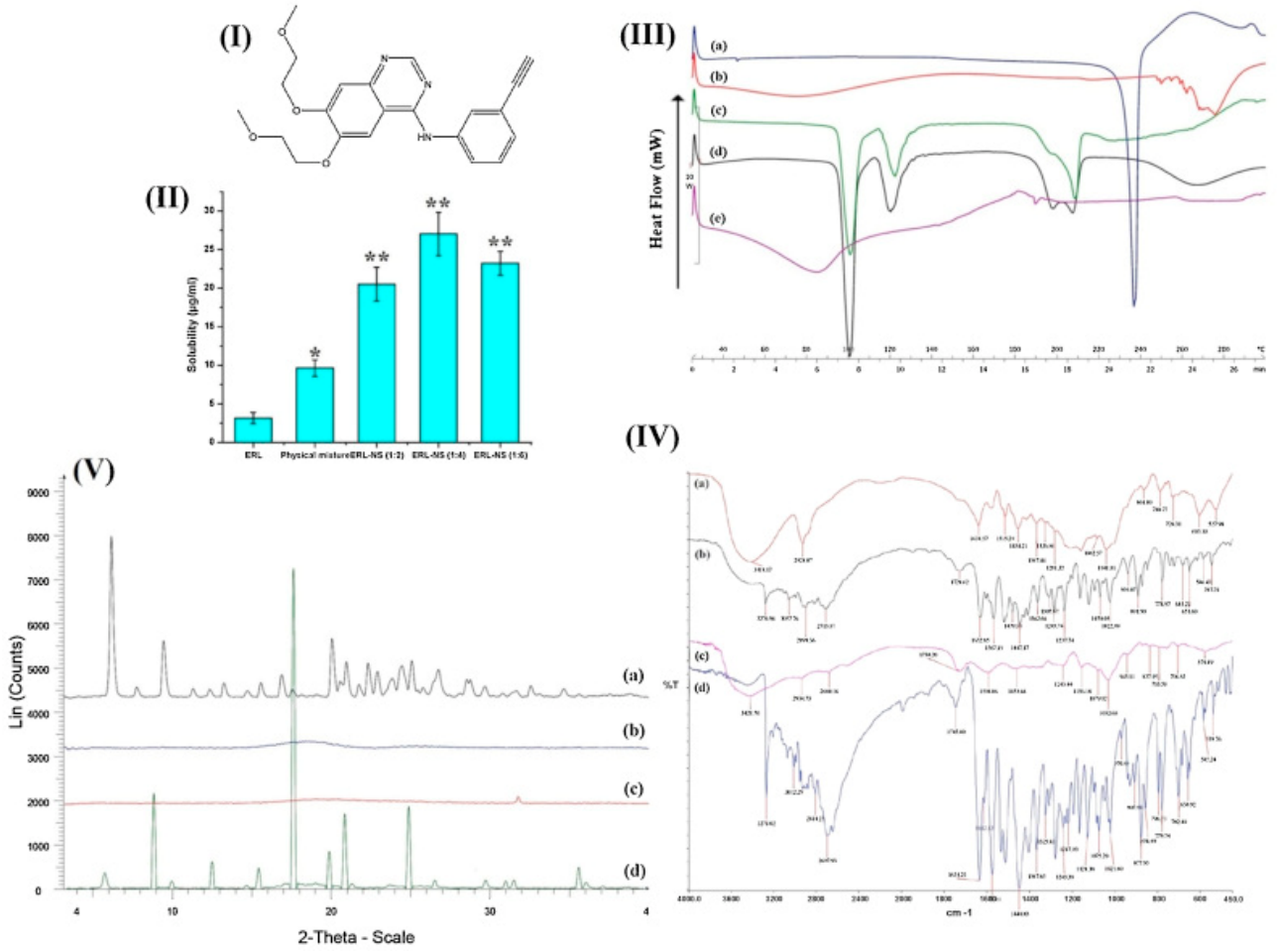

Fig. 1. (I) Chemical structure of Erlotinib. (II) Solubility efficiency of ERL, physical mixture and different ERL-NSs. All values represent data in triplicate (mean ± SD); * indicates $p < 0.05$ and ** indicates $p < 0.001$. (III) DSC thermograms of ERL (a), blank nanosponge (b), Trehalose (c), physical mixture (d), and ERL-NS (e). (IV) FT-IR spectra of ERL-NS (a), physical mixture (b), blank nanosponge (c), and ERL (d). (V) PXRD patterns of ERL (a), Nanosponge (b), ERL-NS (c), and physical mixture (d).

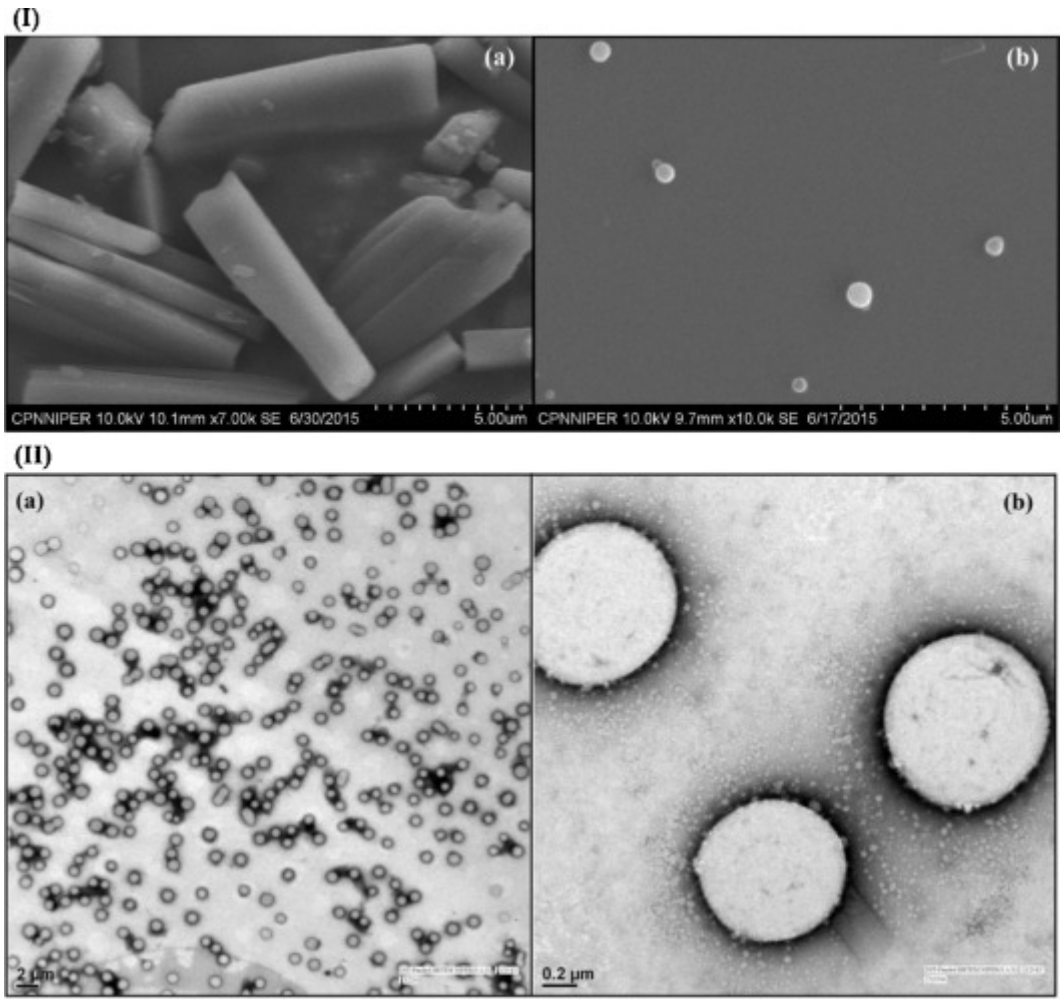

Fig. 2. (I) SEM images of Erlotinib (a), and Erlotinib-Nanosponge complex (b). (II) TEM images of Erlotinib nanosponge complex at different magnifications; (a) X 220 and (b) X 3500.

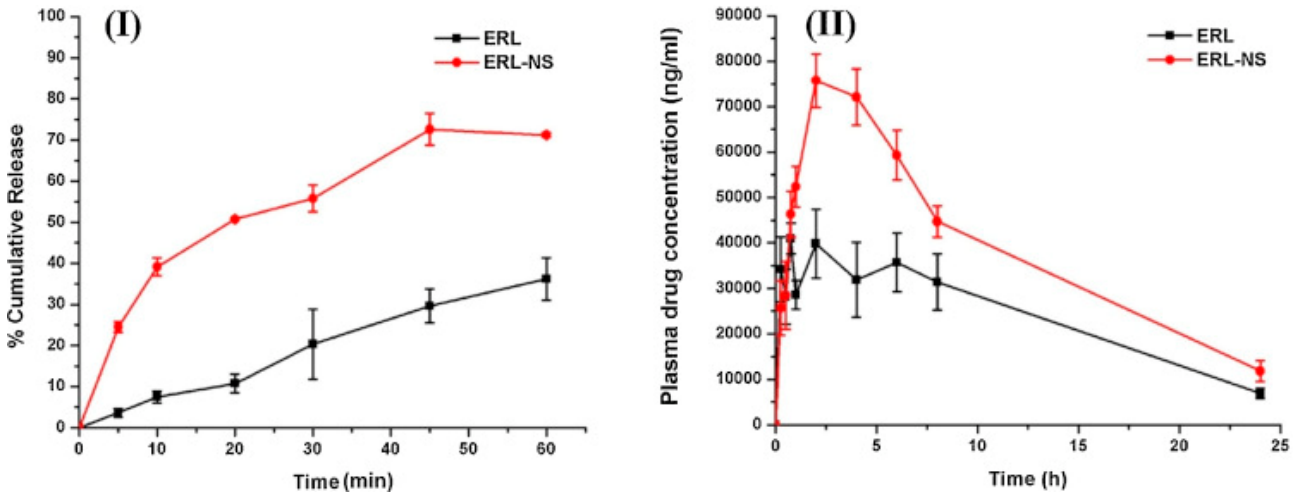

Fig. 3. (I) Dissolution rate profiles of ERL, ERL-Nanosponge complex (mean ± SD; *n* = 3) and (II) *in vivo* pharmacokinetic study of ERL and ERL-nanosponge complex (mean ± SD; *n* = 5).

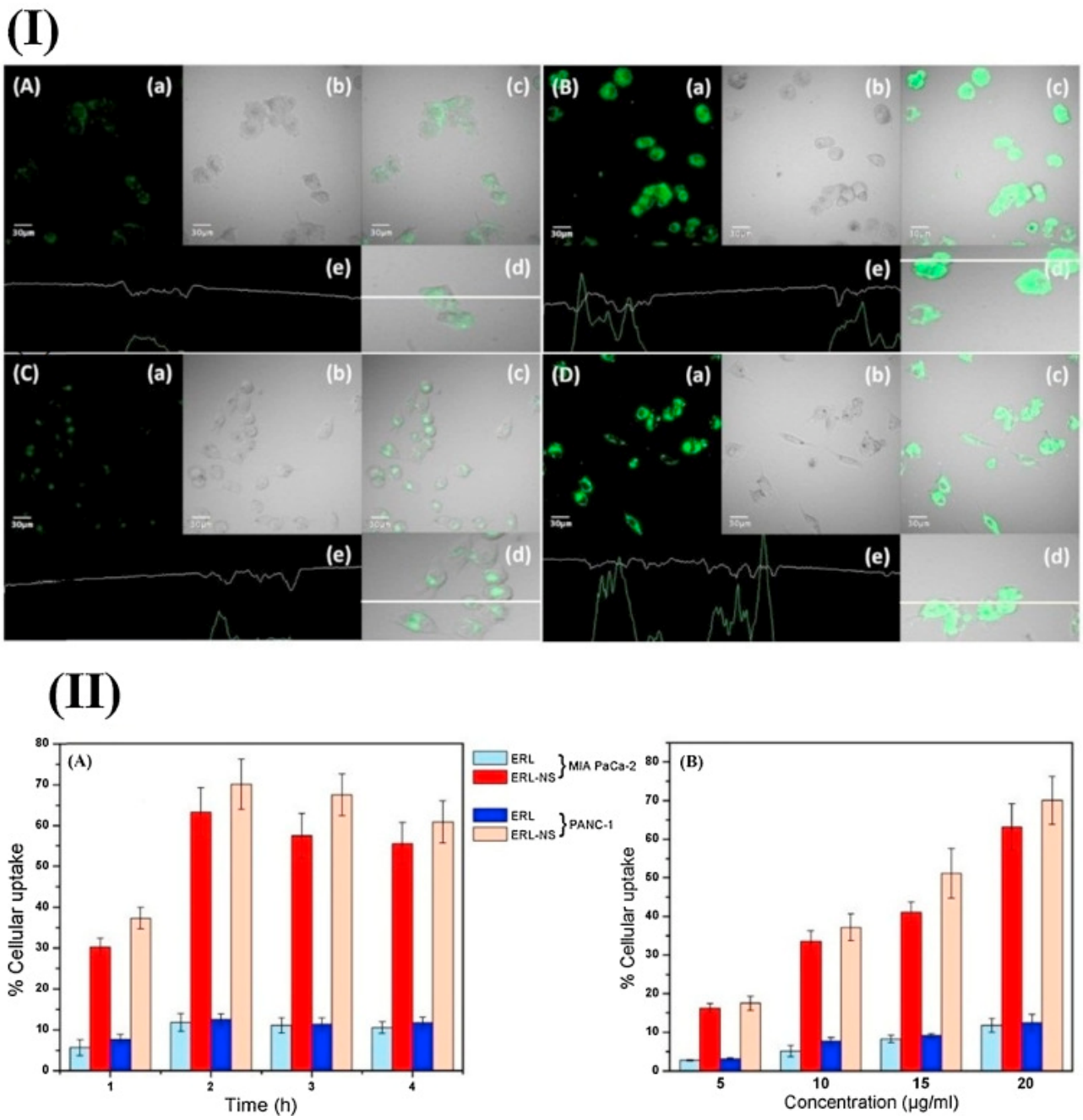

Fig. 4. Mia PaCa-2/PANC-1 cell uptake studies. (I) Qualitative study with PANC-1 cell lines: (A) free Coumarin-6 and (B) Coumarin-6 loaded nanosponge upon incubation at 1 µg/ml for 2 h with PANC-1 cell lines. Qualitative study with Mia PaCa-2 cell lines: (C) free Coumarin-6 and (D) Coumarin-6 loaded nanosponge upon incubation at 1 µg/ml for 2 h with Mia PaCa-2 cell lines. In all the images, (a) The green fluorescence channel; (b) corresponding differential interface contrast images of Mia PaCa-2/PANC-1 cells; (c) superimposition of (a) and (b). (d) and (e) Horizontal line series analysis of fluorescence along the white line. (II) Quantitative study: (A) time dependent and (B) concentration dependent.

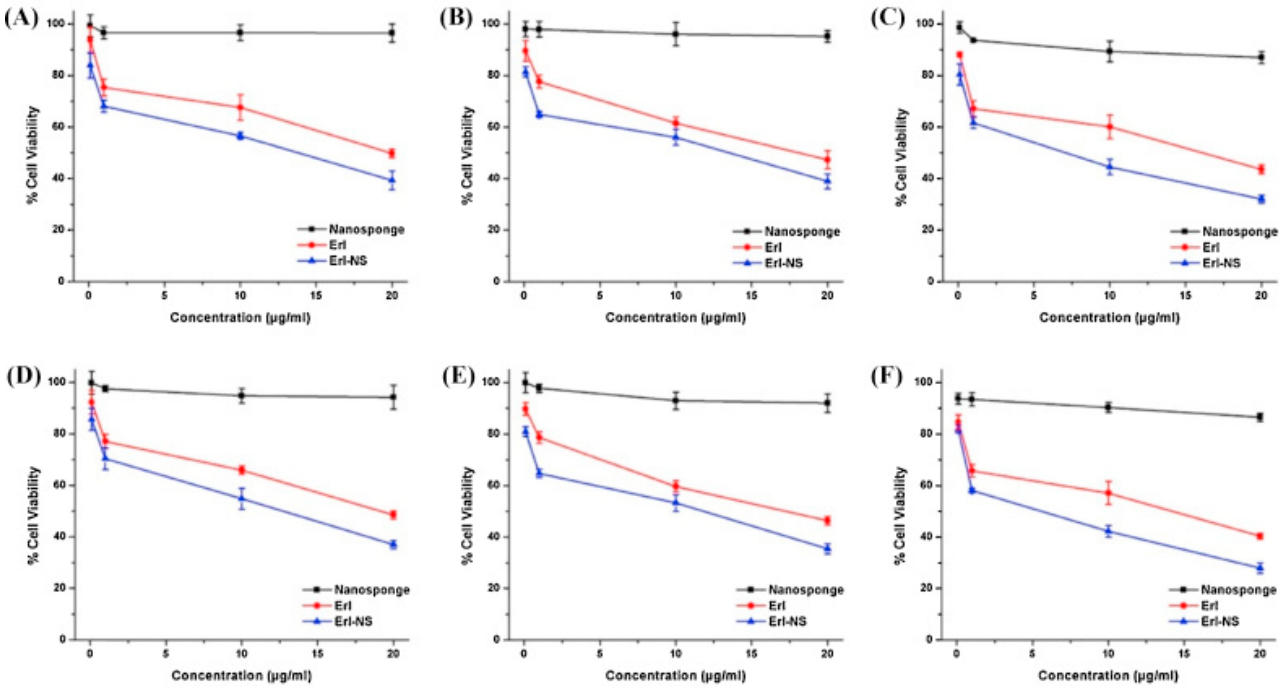

Fig. 5. Cell cytotoxicity of blank nanosponge, ERL and ERL-NS at different concentrations; MIA PaCa-2 studies (24 h (A), 48 h (B), and 72 h (C)), PANC-1 studies (24 h (D), 48 h (E), and 72 h (F)).

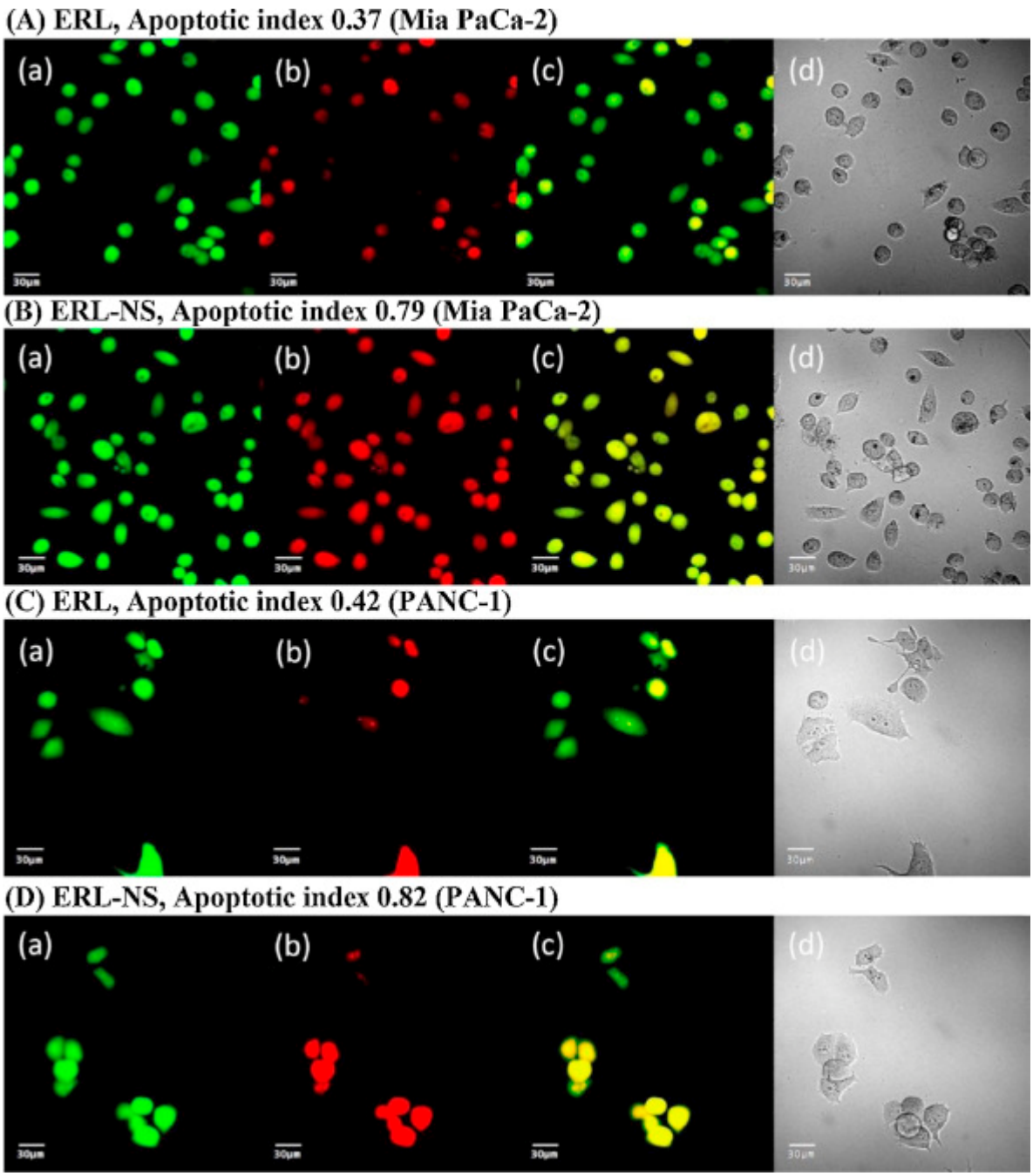

Fig. 6. Apoptosis assay; ERL (A) and ERL-NS (B) with MIA PaCa-2, and ERL (C) and ERL-NS (D) with PANC-1cell lines.

Table 1. Dissolution efficiencies of ERL and ERL-NS.

Sample	Dissolution efficiency		
	DE_{10}	DE_{30}	DE_{60}
ERL	3.70 ± 0.05	9.47 ± 0.14	19.20 ± 0.29
ERL-NS	22.06 ± 1.28*	40.09 ± 3.05*	54.08 ± 3.48*

*p < 0.001 as compared to pure ERL.

Table 2. IC50 values of ERL and ERL-PC at different time points, with different cell lines.

Sample	IC_{50} (µg/ml)					
	Mia-PaCa			PANC-1		
	24 h	48 h	72 h	24 h	48 h	72 h
ERL	18.79	15.11	10.69	18.04	14.28	7.07
ERL-NS	7.28	5.71	2.81	6.23	4.08	2.19

Table 3. In vivo pharmacokinetic parameters of ERL and ERL-NS after single oral administration of 10 mg/kg body weight to rats.

Parameter	Unit	ERL	ERL-NS
$AUC_{0-\infty}$	(µg/ml h)	580.43 ± 71.91	1079.95 ± 41.38*
C_{max}	(µg/ml)	42.36 ± 1.75	78.98 ± 6.2*
T_{max}	(h)	2.7 ± 0.8	2.4 ± 0.4
$T_{1/2}$	(h)	7.9 ± 0.8	8.5 ± 1.35
MRT	(h)	12.8 ± 0.7	12.0 ± 1.8

All values are mean ± SD (n = 5).

*p < 0.001.